J Solid State Electrochem (2012) 16:2019–2029
DOI 10.1007/s10008-012-1751-2

ORIGINAL PAPER

Rechargeable batteries: challenges old and new

John B. Goodenough

Received: 12 March 2012 / Revised: 9 April 2012 / Accepted: 11 April 2012 / Published online: 8 May 2012

Abstract The challenges for rechargeable batteries are cost, safety, energy, density, life, and rate. Traditional rechargeable batteries based on aqueous electrolytes have good rate capabilities but limited energy density because the voltage for a long shelf-life is restricted to 1.5 V. The discovery of fast Na ion conductivity in β-alumina in 1967 introduced the novel concept of a solid oxide electrolyte and molten electrodes: the sodium–sulfur battery operates at 350 °C. Interest in rechargeable batteries with aprotic electrolytes was further stimulated by the first energy crisis in the early 1970s. Since protons are not mobile in aprotic electrolytes, the Li^+ ion was the logical choice for the working ion, and on-going work on reversible Li intercalation into layered sulfides suggested the TiS_2//Li cell, which was shown in 1976 to have a voltage of $V \simeq 2.2$ V and good rate capability. However, the organic liquid carbonates used as electrolytes are flammable, and dendrites growing across the electrolyte from the lithium anode on repeated charge/discharge cycles short-circuited the cells with disastrous consequences. Safety concerns caused this effort to be dropped. However, substitution of the layered oxides $LiMO_2$ for the layered sulfides MS_2 and reversible intercalation of Li into graphitic carbon without dendrite formation at slow charging rates gave a safe rechargeable lithium ion battery (LIB) of large-enough energy density to enable the wireless revolution. Although carbon-buffered alloys now provide anodes that allow a fast charge and have a higher capacity, nevertheless a passivation layer permeable to Li^+ forms on the anode surface, and the Li^+ in the passivation layer is taken irreversibly from the cathode on the initial charge. Since the specific capacity of a cell with an insertion-compound cathode is limited by the latter, strategies to increase the specific capacity for a LIB powering an electric vehicle or storing electricity from wind or solar farms include a return to consideration of a solid electrolyte.

Keywords Electrolyte limits · Electrode voltage/capacity · Charge/discharge rates

Contribution to the symposium: "The Origin, Development, and Future of the Lithium-Ion Battery", University of Texas at Austin, October 22, 2011

J. B. Goodenough (✉)
Texas Materials Institute and the Materials Science and Engineering Program, University of Texas at Austin, Austin, TX 78712, USA
e-mail: jgoodenough@mail.utexas.edu

Introduction

Electrical energy is stored as chemical energy in the electrodes of a rechargeable battery. Cost, safety, the amount of energy stored, battery life, and the power output $P = IV$ of a battery are constraints on the commercial application of batteries.

The output of a battery on discharge is a current $I = dq/dt$ at a voltage V for a time Δt corresponding to a stored energy:

$$\int_o^{\Delta t} IV(t)\mathrm{d}t = \int_o^{Q} V1(q)\mathrm{d}q \tag{1}$$

where the total charge stored

$$Q = \int_o^{\Delta t} I\mathrm{d}t = \int_o^{Q} \mathrm{d}q \tag{2}$$

is the battery capacity. For portable batteries, specific or volumetric energy density (Wh/kg = mAh/g) is a critical parameter. Battery life includes not only shelf-life but also cycle life, defined as the number of charge/discharge cycles before the capacity fades to 80 % of its initial value, i.e., $Q/Q_{in} = 0.8$.

The internal resistance R_b of a battery introduces a voltage polarization loss of $I_{dis}R_b$ on discharge and an overvoltage $\eta = I_{ch}R_b$ on charge, i.e.:

$$V_{dis} = V_{oc} - \eta(q, I_{dis}) \tag{3}$$

$$V_{ch} = V_{oc} + \eta(q, I_{ch}) \tag{4}$$

where V_{oc} is the open-circuit voltage. For stationary storage of electrical energy generated from wind or radiant-solar energy, the storage efficiency:

$$\int_o^Q V(q)_{dis}\mathrm{d}q \Big/ \int_o^Q V(q)_{ch}\mathrm{d}q \tag{5}$$

is also important.

A battery consists of a stack of cells connected in series to increase V_{dis} and in parallel (or electrode area) to increase I_{dis} and/or $\Delta t(I_{dis})$. Of interest for the designer of battery components, particularly the two electrodes and the electrolyte, is the individual battery cell since the parameters of the cell determine the number of cells required for a given application and hence the cost of manufacture and battery management.

Aqueous electrolytes [1]

Figure 1 illustrates the principles of a traditional rechargeable cell having an aqueous electrolyte. The anode is a reductant, the cathode is an oxidant, the separator is an electronic insulator permeable to the electrolyte, and the electrolyte conducts H^+ ions but is an electronic insulator. The separator prevents physical contact between the electrodes inside the cell. The chemical reaction between the anode and the cathode has two components, electronic and ionic. The electrolyte and separator allow the ionic current to flow inside the battery, but they force the electronic component to flow outside the battery through a load resistance R_L where it does useful work. On open circuit, the working ions H^+ flow from the anode to the cathode to charge the cathode positively and the anode negatively until the electrochemical potentials of the two electrodes are equal; V_{oc} is the resulting voltage difference between the two electrodes. On discharge, electrons and H^+ ions flow from the anode to the cathode until the chemical reaction is complete; on charge, these current flows are reversed by the application of a charging voltage $V_{ch} > V_{dis}$.

The V_{oc} of a rechargeable battery is determined by the "window" of the electrolyte. As illustrated in Fig. 2, the electrolyte window is the electron energy gap E_g = LUMO − HOMO, where LUMO is the energy of the lowest unoccupied molecular orbital of the electrolyte and HOMO is the energy of the highest occupied molecular orbital. An anodic electrochemical potential μ_A > LUMO can reduce the electrolyte; a cathodic electrochemical potential μ_C < HOMO can oxidize the electrolyte. In an aqueous electrolyte, E_g = 1.23 eV separates the H_2O/H_2 LUMO and the O_2/H_2O HOMO. However, a kinetic stability, owing to an energy barrier for electron transfer between electrode and electrolyte, can allow a room-temperature $V_{oc} \simeq 1.5$ V where μ_A and μ_C are well-matched, respectively, to the aqueous LUMO and HOMO. For example, the nickel–cadmium rechargeable cell has an alkaline electrolyte (KOH) and a V_{oc}=1.5 V. The anode undergoes the displacement reaction:

$$Cd^0 + 2H_2O = Cd(OH)_2 + 2H^+ + 2e^- \tag{6}$$

and the cathode the hydrogen insertion reaction:

$$NiOOH + H^+ + e^- = Ni(OH)_2 \tag{7}$$

On the other hand, an electrode with a μ_A > LUMO or a μ_C < HOMO may be stabilized by an electrode–electrolyte reaction that generates a passivating layer on the surface of the electrode that does not block cation migration through it. For example, the lead acid cell has an acidic electrolyte (H_2SO_4) and a $V_{oc} \simeq 2.0$ V. In this cell, the anode and the cathode reactions are:

$$Pb^0 + H_2SO_4 = PbSO_4 + 2H^+ + 2e^- \tag{8}$$

$$PbO_2 + H_2SO_4 + 2e^- = PbSO_4 + 2H_2O \tag{9}$$

followed by slow dissolution of the passivating $PbSO_4$ layer. Removal of the passivation layer is responsible for the limited life of the lead acid battery.

Solid electrolytes

Since the volumes of the two electrodes change during discharge and charge, a solid–solid interface between a solid electrolyte and a large-capacity solid electrode generally has a limited life. Therefore, a solid electrolyte in a large-capacity rechargeable battery is best used with liquid or gaseous electrodes. Moreover, a relatively large enthalpy of ion motion in a solid has restricted use of solid electrolytes to high-temperature electrochemical cells compatible with molten or gaseous electrodes.

The discovery in 1967 of fast 2D Na^+ ion transport in ß-Al_2O_3 by Kummer and Weber [2] and their suggestion of the sodium–sulfur battery marked a turning point in the strategic thinking about rechargeable batteries. The cell of

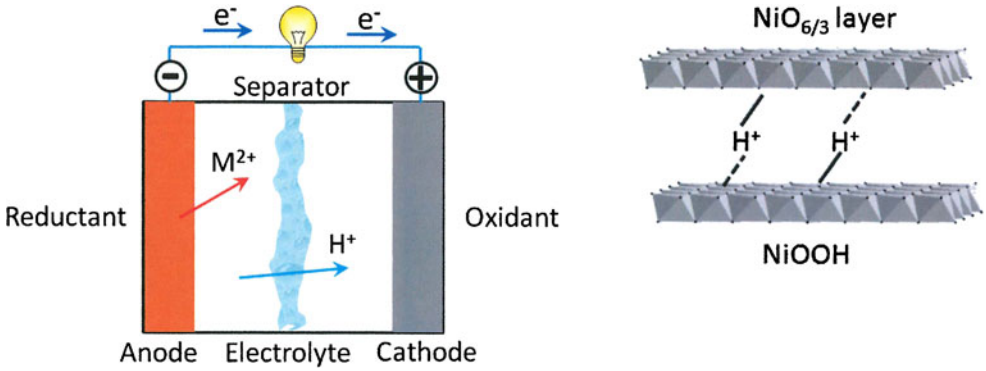

Fig. 1 Traditional rechargeable cell and layered NiOOH structure

a sodium–sulfur battery [3] (Fig. 3) uses molten sodium as the anode and molten sulfur impregnated with carbon felt for electron transfer as cathode; it operates near 350 °C with, as electrolyte, a solid ceramic composite of ß,ß"-Al_2O_3 toughened by incorporation of particles of ZrO_2. The development of the sodium–sulfur battery, now operational in Japan, stimulated work on the Zebra battery [4], which replaces the molten sulfur cathode with molten $NiCl_2$ and is fabricated in the discharged state with Ni dispersed in molten $NaCl_2$. Where the reaction Na + S = NaS gives a V_{oc}=2.0 V, the reaction 2Na + $NiCl_2$=2NaCl + Ni gives a V_{oc}=2.58 V at 350 °C.

A solid oxide fuel cell uses an oxide ion solid electrolyte that transports oxide ions from the cathode to the anode during discharge. The anode catalyzes the oxidation of H_2 by the reaction

$$H_2(g)+O^{2-}(s)=H_2O(g)+2e^- \quad (10)$$

The cathode catalyzes the oxygen reduction reaction

$$1/2O_2(g)+2e^-=O^{2-}(s) \quad (11)$$

The operating temperature 600 °C < T_{op}<1,000 °C for a desired output power depends on the electrode and electrolyte materials used. In an electrolysis mode, all the reactions would be reversed with the cathode catalyzing the oxygen evolution reaction. The cell becomes a solid oxide electrochemical cell (SOEC) when used in the fuel cell mode on discharge and the electrolysis mode on charge. The group of Kevin Huang [5] has recently demonstrated a novel solid oxide redox flow battery (SORFB) of potential for grid energy storage that uses existing SOEC technology and, though operating at higher temperature, can compete economically with the sodium–sulfur and Zebra batteries. The SORFB (Fig. 4) consists of a SOEC coupled to an Fe/FeO_x or other redox bed through which the product gases of the anode of the SOEC are circulated. During discharge, steam from the anode reaction (10) reacts with Fe in the redox bed:

$$Fe+xH_2O = FeO_x+H_2 \quad (12)$$

to continue feeding H_2 to the anode until nearly all the Fe is converted to FeO_x. The SOEC is then switched to the electrolysis mode where reactions (10) and (12) are reversed to recharge the redox bed from FeO_x to Fe. With reaction (11), the overall chemical reaction of the

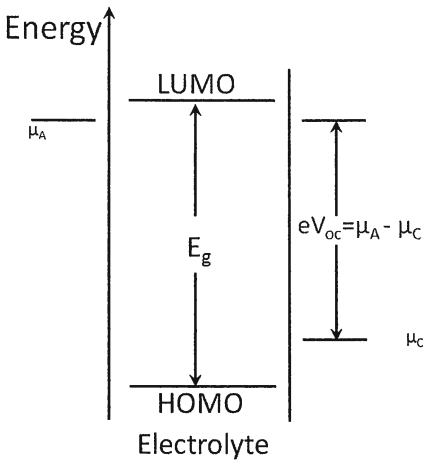

Fig. 2 Electrode electrochemical potentials versus window, E_g, of the electrolyte

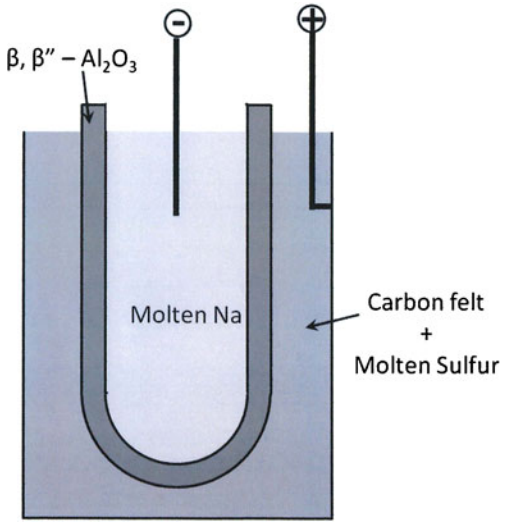

Fig. 3 The sodium–sulfur cell

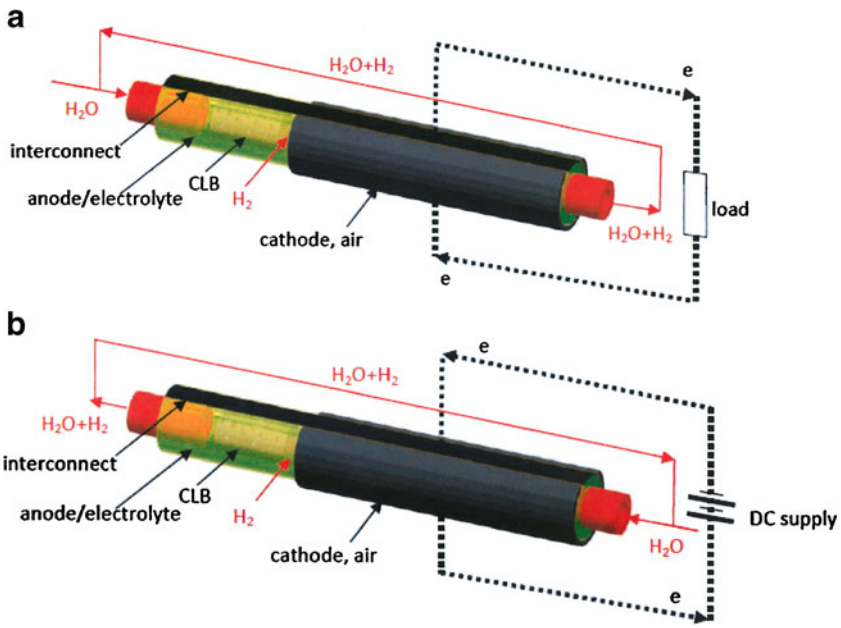

Fig. 4 The solid-oxide redox-flow battery: **a** discharge, **b** charge modes

SORFB becomes

$$\mathrm{Fe} + \frac{x}{2}\mathrm{O_2} \frac{\leftarrow \text{Charge}}{\text{Discharge} \rightarrow} \mathrm{FeO}_x \tag{13}$$

A nearly 92 % cycle efficiency has been demonstrated. Among the several advantages of this scheme are a Nernst potential controlled by the two-phase thermodynamic Fe/FeO_x equilibrium, self-sustaining thermal management, and a free-standing redox displacement reaction having its volume changes decoupled from the structured components of the SOEC.

Organic liquid electrolytes [6]

An aprotic liquid electrolyte with a larger window than water would enable the design of a room-temperature cell with a higher voltage, but the only known liquid in which H^+ ions are mobile is water. The Li^+ ion is, like H^+, small and light; moreover, lithium offers the highest anodic electrochemical potential energy μ_A. Lithium salts can be dissolved dissociatively into relatively non-viscuous organic carbonates to give a Li-ion conductivity $\sigma_{Li} > 10^{-2}$ S cm^{-1}. With an ethylene carbonate additive, these Li^+ carbonate electrolytes form a solid electrolyte interphase (SEI) layer on lithium that is permeable to Li^+ ions [7]. The availability of an aprotic Li^+ liquid electrolyte stable against a lithium anode appeared to open up the possibility of a Li-ion rechargeable battery provided that a reversible cathode could be found.

Layered sulfide cathodes

In the early 1970s, Schöllhorn [8] in Germany and Rouxel [9] in France were exploring the chemistry of reversible Li intercalation into the Van der Waals gap of layered transition metal sulfides (Fig. 5). Both TiS_2 and VS_2, for example, have cations in alternate octahedral-site layers of a hexagonal close-packed sulfide-ion sublattice; the strongly bonded layers of edge-sharing octahedra are held together by weak Van der Waals bonding. Given the reversible proton insertion between the NiO_2 layers of the NiOOH cathode of the nickel–cadmium cell (Fig. 1), the layered sulfides became natural cathode candidates for a rechargeable Li-ion battery. In 1976, Whittingham [10] reported a rechargeable TiS_2//Li cell having an excellent rate capability and a capacity comparable to that of the nickel–cadmium cell with a $V_{oc} \simeq 2.2$ V. However, the SEI layer on the lithium anode causes a mossy Li deposit during charge, and on repeated cycling, dendrite growth from the anode across the electrolyte began to short-circuit cells with explosive or incendiary consequences. Since a safe alternative anode would lower the voltage to where a battery with a layered sulfide cathode would not be competitive with existing rechargeable batteries, this effort to develop a Li ion rechargeable battery was abandoned.

Layered oxide cathodes

By 1978, it was apparent to me that the problem with the layered sulfides as cathodes was an energy of the top of the S-3p bands that was too high to allow a $V_{oc} > 2.6$ V versus Lithium, which is not competitive if the anode μ_A needs to be lowered from that of lithium. However, the top of the O-2p bands would be at a lower energy than the top of the S-3p

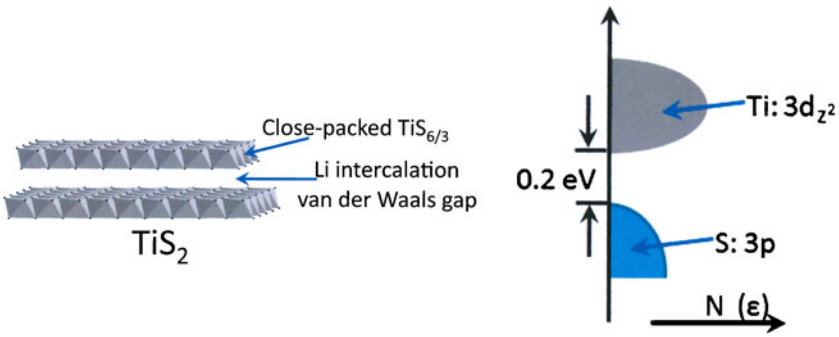

Fig. 5 Layered TiS_2: structure and one-electron energy densities N(E)

bands. Although layered oxides similar to the layered sulfides do not exist, I also knew that the oxides $LiMO_2$ can order Li^+ and M^{3+} ions into alternate (111) planes of a face-centered-cubic oxide-ion sublattice. Therefore, I assigned a visiting scientist, Koichi Mizushima, to work with my postdoc Phillip Wiseman and a student P.C. Jones to explore the extent of reversible extraction of Li from layered $LiMO_2$ oxides as opposed to reversible Li insertion into MS_2 sulfides [11]. In 1980, we reported a $V_{oc} \simeq 4.0$ V for $Li_{1-x}CoO_2$ in the compositional range $0 \leq \times \leq 0.5$. We followed [12] with a similar result at a $V_{oc} \simeq 3.8$ V for $Li_{1-x}NiO_2$. We also showed [13] that the Li^+ mobility in the oxide was superior to that in TiS_2. However, in the absence of a safe discharged anode, no battery company was interested in our layered oxide cathodes.

At the same time, chemists were interested in intercalation of Li into graphite [14], and in 1983, Yazami and Touzain [15] reported a reversible Li intercalation into a graphite anode. At low charging rates, this anode is not plagued by Li plating on the anode surface with subsequent dendrite growth on repeated cycling. Yoshino [16] then realized that charging the graphitic anode with Li from a discharged $LiCoO_2$ cathode would give a safe, high-energy-density Li-ion rechargeable battery. SONY Corporation of Japan used this cell (illustrated schematically in Fig. 6) to market the first cell telephone and launch the wireless revolution.

The $Li_{1-x}CoO_2$ cathode is preferred over the $Li_{1-x}NiO_2$ cathode because $LiCoO_2$ has a better ordering of the Li^+ and

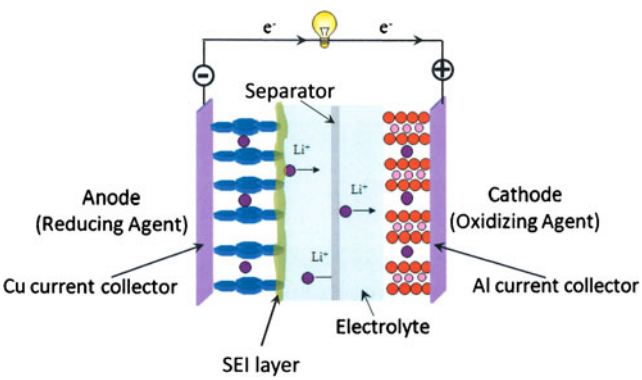

Fig. 6 The $LiCoO_2$//C cell

Co^{3+} ions. However, the top of the O-2p bands about 4 eV below μ_A of lithium limits the capacity of $Li_{1-x}CoO_2$ to $0 \leq x \leq 0.55$ and of $Li_{1-x}NiO_2$ to $0 \leq x \leq 0.8$. For larger x, peroxide ions are formed on the cathode surface with subsequent loss of O_2 and/or insertion of hydrogen atoms from the electrolyte [17]. The loss of O_2 from the cathode reflects the intrinsic voltage limit of these layered oxides; the insertion of hydrogen appears to reflect the presence of some water in the electrolyte. On the other hand, electrolyte decomposition above 5 V versus lithium [18] is initiated at voltages $V > 4.0$ V, but kinetic stability at an oxide cathode is generally found for $V < 4.5$ V versus lithium, which makes difficult the definition of the HOMO energy within the range $4.0 < \text{HOMO} < 4.3$ eV below μ_A (Li^0).

Electrode limitations on energy density

The capacity of an insertion-compound electrode is limited by the solid-solution range of the guest Li in the host structure. Moreover, if the anode has a μ_A above the electrolyte LUMO, it must be stabilized by the formation of an SEI passivation layer that is permeable to Li^+ ions. In this case, an *irreversible* loss of Li from the limited capacity of the cathode is encountered on the initial charge of a battery assembled with a discharged cathode.

As shown in Fig. 7, the LUMO of a carbonate electrolyte is located about 1.1 eV below μ_A (Li^0). Therefore, a graphite anode, which has a $\mu_A \simeq 0.2$ eV below μ_A (Li^0), is passivated by an SEI layer, for example. Moreover, a fast charge may require a V_{ch} high enough to plate lithium on the surface of the carbon more rapidly than Li^+ ions can permeate the SEI layer, which is why the rate of charge is limited with a graphite electrode. On the other hand, introduction of an alloy with a $\mu_A > 0.5$ eV below μ_A (Li^0) can both increase the anode capacity and allow fast charge [19], but a good cycle life then requires buffering the large alloy volume change with carbon. Nevertheless, an anode with a $\mu_A >$ LUMO will rob Li *irreversibly* from the cathode on the initial cell charge.

Limitations on the cathode voltage are imposed by the electrolyte HOMO if not by an intrinsic limitation. The voltage of the TiS_2 cathode can be seen in Fig. 7 to be

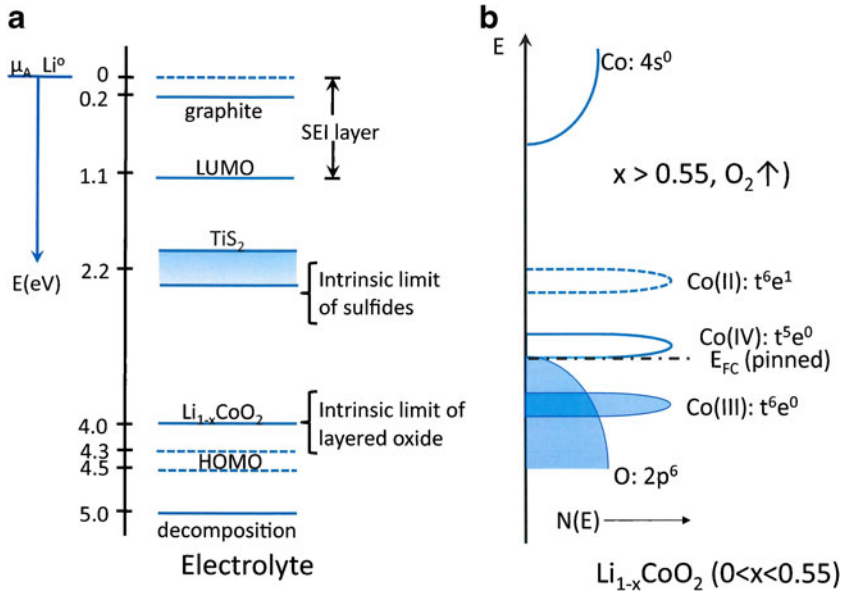

Fig. 7 **a** Electrode energies and liquid-carbonate electrolyte window versus lithium. **b** Illustration of pinning of μ_C of Co (IV)/Co(III) at top of O-2p bands

poorly matched to the carbonate HOMO; in a recent study, we [20] have demonstrated that the intrinsic voltage limit of a layered sulfide is about 2.6 eV below μ_A (Li^0). The μ_C of $Li_{1-x}CoO_2$, on the other hand, is better matched to the carbonate HOMO, but the intrinsic voltage limit restricts the capacity. The intrinsic voltage limit of a cathode occurs where μ_C is pinned at the top of the anion-p bands [21]. This phenomenon is illustrated in Fig. 7 for $Li_{1-x}CoO_2$. As the energy of the *d*-electron redox couple is lowered across the top of the O-2p bands, holes introduced by oxidation of the couple occupy antibonding states at the top of the bonding O-2p states. The holes occupy states that retain the symmetry of the cation *d*-electron states, but the fraction of anion-p character in the hole states increases as the redox couple is lowered and/or the hole concentration increases; the O-2p character of the states becomes dominant where the couple crosses the top of the O-2p bands. At a critical fraction of anion-p character, the holes become trapped in surface dianion molecules, e.g., peroxide $(O_2)^{2-}$ on an oxide surface. The peroxide ions readily lose gaseous O_2 in the reaction:

$$2(O_2)^{2-} = 2O^{2-} + O_2 \uparrow \tag{14}$$

Spinel hosts

In 1981, CSIRO of South Africa sent Michael Thackeray to my laboratory at Oxford to explore the insertion of Li into the less costly oxospinel Fe_3O_4. I knew that it is not possible to introduce interstitial cations into a spinel. As can be seen from the structure (Fig. 8), the interstitial *16d* octahedral sites share common faces with the tetrahedral *8a* cation sites, making the cation–cation Coulomb interactions across a shared face too strong for stability. Nevertheless, Thackeray did insert Li into Fe_3O_4, and we quickly learned from the X-ray data of my postdoc Bill David that the inserted Li displaced in a cascade all the tetrahedral-site Fe of Fe_3O_4 into the interstitial 1*6d* octahedral sites to form a semi-ordered rock-salt structure with the $[Fe_2]O_4$ spinel framework intact [22]. With the realization that the $[M_2]O_4$ array of a spinel offers an oxide host with a 3D interstitial space in which Li^+ ions are mobile, I told Thackeray to insert Li into the spinel $Li[Mn_2]O_4$. He subsequently showed reversible Li insertion into $Li[Mn_2]O_4$ with a $V_{oc} \simeq 3.0$ V versus lithium [23], and on his return to South Africa, he showed that Li extraction gives a $V_{oc} \simeq 4.0$ V despite working on the same Mn^{4+}/Mn^{3+} redox couple [24] (see Fig. 8). The shift of the Li from tetrahedral to octahedral sites changes the energy of the Mn^{4+}/Mn^{3+} couple by 1 eV, which halves the useful capacity. Nevertheless, a rapid and reversible 3D insertion of Li into a spinel framework was established, and Thackeray's group [25] subsequently patented the spinel $Li_{1+x}[Li_{1/3}Ti_{5/3}]O_4$ as a stable anode with a $V_{oc} \cong 1.5$ V versus lithium, a safe 0.4 eV below the LUMO of the carbonate electrolytes.

A more subtle change in the $V(x)$ curve of Fig. 8 occurs at x=0.5 of $Li_x[Mn_2]O_4$. The tetrahedral *8a* sites form a diamond-like sublattice consisting of two interpenetrating face-centered-cubic subarrays. At x=0.5, the Li^+–Li^+ interactions stabilize an ordering of the Li^+ ions on one of the two subarrays to create a Li-poor and a Li-rich two-phase region in the interval $0<x<0.5$. The flat $V(x)$ =3.0 V in the range $1<x<1.8$ is caused by a cooperative Jahn–Teller orbital ordering on Mn^{3+} ions that stabilizes a Li-rich tetragonal phase and a Li-poor cubic phase. Complications arising from Li^+ ion ordering at x=0.5 as well as from cooperative

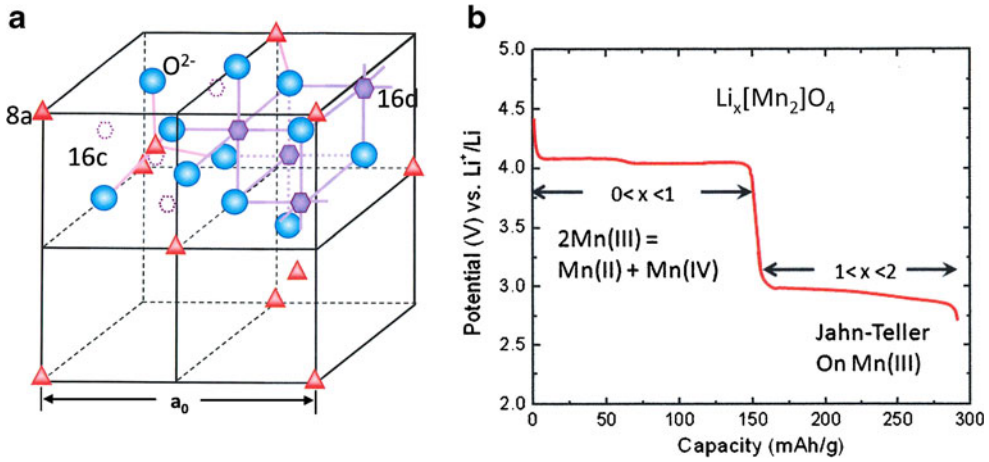

Fig. 8 **a** Two quadrants of the cubic spinel structure, **b** $V(x)$ profile $Li_x[Mn_2]O_4$

Jahn–Teller ordering and the surface disproportion reaction $2\ Mn^{3+}=Mn^{2+} + Mn^{4+}$ followed by dissolution of Mn^{2+} into the electrolyte have plagued exploitation of the $V_{oc}\approx$ 4.0 V of a $Li_{1-x}[Mn_2]O_9$ cathode [26]. However, mixing into the spinel a compound containing only Mn^{4+} ions, e.g. $Li(Ni_{0.5}Mn_{1.5}]O_4$, disrupts ordering at x=0.5, dilutes the Mn^{3+} concentration in the bulk, and suppresses disproportionation at the surface to give an acceptable cycle life.

Interestingly, the substitution $Mn^{4+} + Ni^{2+}=2\ M^{3+}$, not only in the spinel but also in the layered structure, stabilizes the top of the O-2p bands to 4.8 V to allow oxidation of all the nickel from Ni^{2+} to Ni^{4+} in the range 4.6<4.8 V versus lithium with no significant voltage step between the Ni^{3+}/Ni^{2+} and Ni^{4+}/Ni^{3+} couples [27]. The O-2p fraction in the hole states of both redox couples is sufficient to make the holes itinerant. Above 4.8 V, oxygen is evolved. On the other hand, the substitution $Ti^{4+} +Ni^{-2+}=2\ M^{3+}$ has an opposite effect; it suppresses access to even the Ni^{3+}/Ni^{2+} couple [28].

Frameworks with $(XO_4)^{n-}$ anions

The discovery of 2D Na^+ ion transport in ß-Al_2O_3 led me to search for 3D Na^+ ion conduction in framework structures [29]. The best of these, $Na_{1+3x}Zr_2(P_{1-x}Si_xO_4)_3$ with x≈2/3, was developed with Henry Hong [30] in 1976 while I was at MIT Lincoln Laboratory; its framework has the hexagonal $Fe_2(SO_4)_3$ structure of Fig. 9. The compound was later identified by colleagues as NASICON, i.e., a NA SuperIonic Conductor. In 1988, I suggested to my new postdoc, Arumugam Manthiram, that he investigate Li insertion into the hexagonal $Fe_2(XO_4)_3$ frameworks with X=S, Mo, or W. Manthiram [31] showed that the voltage of these compounds jumps from $V_{oc}\approx$3.0 V with X=Mo or W to 3.6 V versus lithium with X=S. This experiment demonstrated the influence, through the inductive effect, of the counter cation X on the energy of the Fe^{3+}/Fe^{2+} couple just as shifting of Li^+ from tetrahedral to octahedral sites at x=1.0 in $Li_x[Mn_2]O_4$ changes the energy of the Mn^{4+}/Mn^{3+} redox couple by 1 eV. This observation led me to give as a dissertation topic to my Ph.D. student, Ashoka Padhi, a comparison of the redox energies of different redox couples in NASICON frameworks with $(SO_4)^{2-}$ and $(PO_4)^{3-}$ anions. With my postdocs, Kirakodu Nanjudaswami and Christian Masquelier, and a visiting scientist, Shigeto Okada from Nippon Telephone and Telegraph of Japan, mapping of the redox energies [32] showed a general lowering of about 0.8 eV of all the redox energies on charging from $(PO_4)^{3-}$ to $(SO_4)^{2-}$. The Fe^{3+}/Fe^{2+} couple in $Li_{3+x}Fe_2(PO_4)_3$ gives 2.8 V versus lithium as against 3.6 V in $Li_xFe_2(SO_4)_3$, for example. In this framework, the couples are not sensitive to the Li^+ concentration. The V^{4+}/V^{3+} couple of hexagonal $Li_{3-x}V_2(PO_4)_3$ gives 3.7 V versus lithium. While exploring the M^{3+}/M^{2+} redox energies in the spinels $V[LiM^{2+}]O_4$, Padhi found that he could not access Fe^{2+} in these spinels. When I explained to him that the Fe^{3+}/Fe^{2+} couple has a higher energy than the

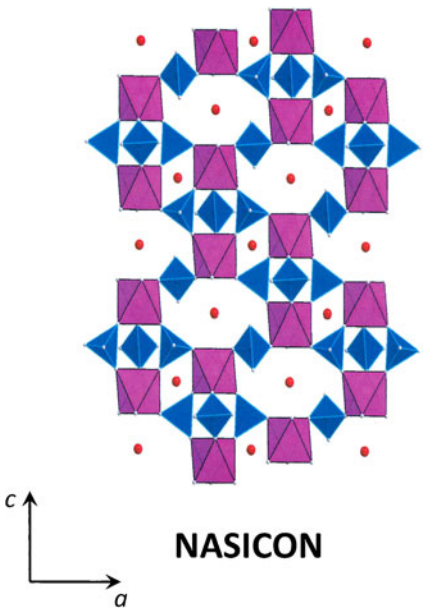

Fig. 9 The $M_2(XO_4)_3$ NASICON framework structure

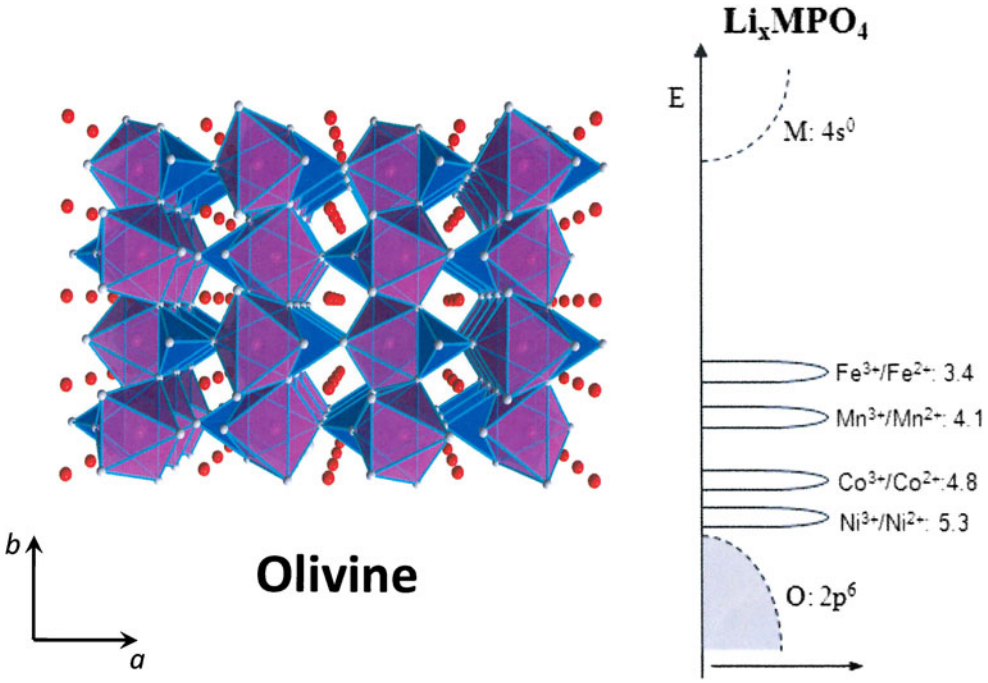

Fig. 10 The structure of the ordered olivine $LiFePO_4$

V^{5+}/V^{4+} couple, he decided to substitute PO_4 for VO_4, which gave him the ordered olivine $LiFePO_4$ of Fig. 10 [33].

$LiFePO_4$ has only 1D channels for Li^+ transport and a small but first-order deformation of the $FePO_4$ framework between $LiFePO_4$ and $FePO_4$, which gives a flat $V(x)$= 3.45 V profile versus lithium in the range 0<x<1. Although the electronic conductivity is poor and the Li^+ move in 1D channels, small particles form as flat plates with the 1D channels perpendicular to the plate surface [34]. Moreover, the group of Michel Armand [35], while he was at the University of Montréal, Canada, showed that lithiating small particles of $FePO_4$ with a carbon precursor gives a carbon coat permeable to Li^+ that provides the needed electronic conduction. The voltage of this carbon-coated cathode lies within the window of the carbonate electrolytes; in a review, Karim Zaghib et al. [36] have provided evidence that it can provide a safe, high-power battery with long cycle life. Batteries with $LiFePO_4$ cathodes have been successfully marketed. Moreover, from the mapping of redox energies in the NASICON framework, it was shown that $LiMnPO_4$ has a $V_{oc} \simeq 4.1\,V$ versus lithium and it has been possible to predict that $LiCoPO_4$ should have a $V_{oc} \simeq 4.8\,V$ and $LiNiPO_4$ a $V_{oc} \simeq 5.3\,V$ versus lithium, but rapid extraction of Li from $LiMnPO_4$ and $LiCoO_4$ has proven to be challenging because of a different face of the particle platelets, and the cost of cobalt as well as a voltage outside the window of the carbonate electrolyte has prevented extensive work on $LiCoPO_4$.

Although these studies with the liquid-carbonate electrolytes have resulted in the wireless revolution, the present worldwide race to develop inexpensive rechargeable power batteries of high energy density and long cycle life for electric vehicles and for large-capacity storage of electric energy generated by wind and/or solar energy confronts a major challenge, viz: *how to increase the cell capacity beyond what is possible with an insertion-compound cathode.*

Return to solid electrolytes

High-capacity batteries have been demonstrated with a solid Na^+ ion electrolyte and molten electrodes operating at 350 °C as well as with an oxide ion solid electrolyte with flow-through gases over a redox bed operating above 600 °C. These batteries show that alternatives to solid cathodes into which Li is inserted reversibly can give higher cell capacities and that solid electrolytes can enable these strategies. Moreover, the observation of fast Li insertion into solid cathodes with close-packed oxygen or sulfur arrays indicates that Li^+ ion solid electrolytes having a 3D Li^+ conductivity $\sigma_{Li} > 10^{-3}$ S cm^{-1} may be achieved in crystalline sulfides as well as in sulfide glasses and, perhaps, also in crystalline oxides. Whereas an all-solid-state battery of high capacity does not appear to be feasible, a solid–solid interface between a Li anode and a solid electrolyte might be reversible. Moreover, a cell with a Li^+ ion solid electrolyte as separator can be envisaged as cartooned in Fig. 11. A lithium anode could then be used with a liquid-carbonate or gel electrolyte on the anode side of the separator; the Li^+ of the SEI layer formed on the anode would come from the anode itself, not the cathode, and dendrites would be blocked by the solid electrolyte separator. On the cathode side, a liquid or gaseous cathode could be used as well as a

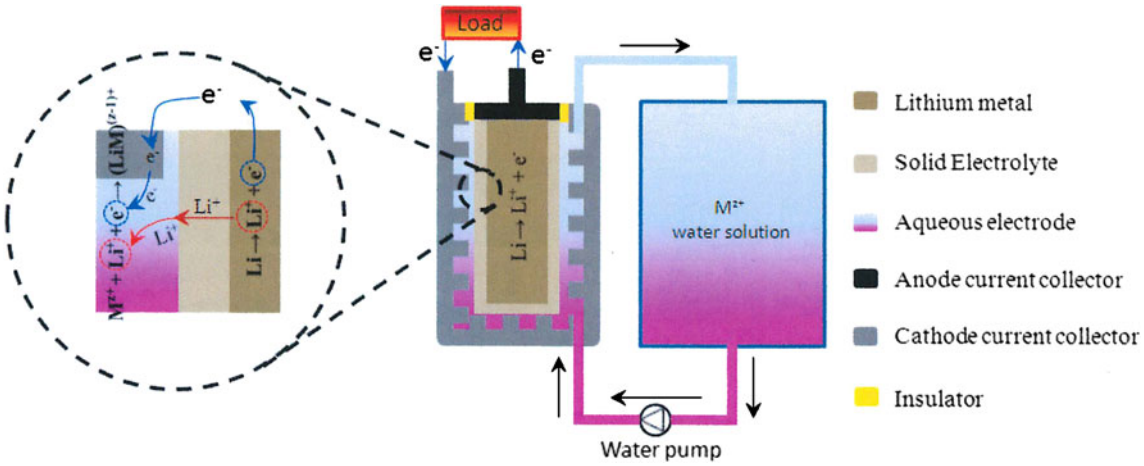

Fig. 11 A possible configuration for a cell having a Li^+ ion solid electrolyte separator

solid insertion compound, and with a solid cathode, an alternative to the liquid-carbonate electrolyte having a HOMO > 5 eV below μ_A (Li^0) could be used to allow a higher cathode voltage than 4.5 V without an SEI layer.

As an alternative to an insertion compound on the cathode side, a room-temperature liquid like bromine in metallic foam could be used as the cathode just as is molten sulfur in a carbon felt in the sodium–sulfur battery. A solid displacement reaction on the cathode side would need to be buffered by carbon to accommodate the large volume charges on cycling as has been demonstrated for a solid sulfur cathode assembled as discharged Li_2S in carbon. Massoun and Scrosati [37] have documented reversible cycling with this cathode in a liquid-carbonate gel electrolyte, but with this cathode, a lithium anode is needed to give an adequate voltage.

Other strategies could involve an aqueous solution on the cathode side, but these strategies require an oxide Li^+ ion solid electrolyte. For example, an air cathode is not reversible with an organic electrolyte [38], but in an alkaline aqueous electrolyte with proper oxide catalysts, reversible air electrodes have been demonstrated with only 0.3 V separating one oxygen reduction reaction on discharge and the oxygen evolution reaction on charge [39]. In another direction, we have demonstrated the feasibility, in principle, of a liquid flow-through cathode consisting of the $Fe(CN)_6^{3-}/Fe(CN)_6^{4-}$ couple in an alkaline aqueous solution [40]. However, the iron cyanide solution does not retain a strongly alkaline pH on cycling, so this strategy may require an acidic host to prevent competition between Li^+ and H^+ for occupancy of the electrolyte host framework.

The strategies outlined above depend upon the identification of a suitable Li^+ ion solid electrolyte. Kamaya et al. [41] have reported a room-temperature $\sigma_{Li} \simeq 1.2 \times 10^{-2}$ S cm^{-1} in the sulfide Li^+ ion conductor $Li_{10}GeP_2S_{12}$, but matching the anode μ_A to the LUMO will need to be explored as its HOMO is expected to be below μ_A (Li^0). At the present time, the most promising Li^+ ion solid electrolyte has a garnet framework [42] as host with a room-temperature $\sigma_{Li} \simeq 10^{-3}$ S cm^{-1}, but this framework is basic, requiring the retention of a pH>12 if an aqueous cathode is used.

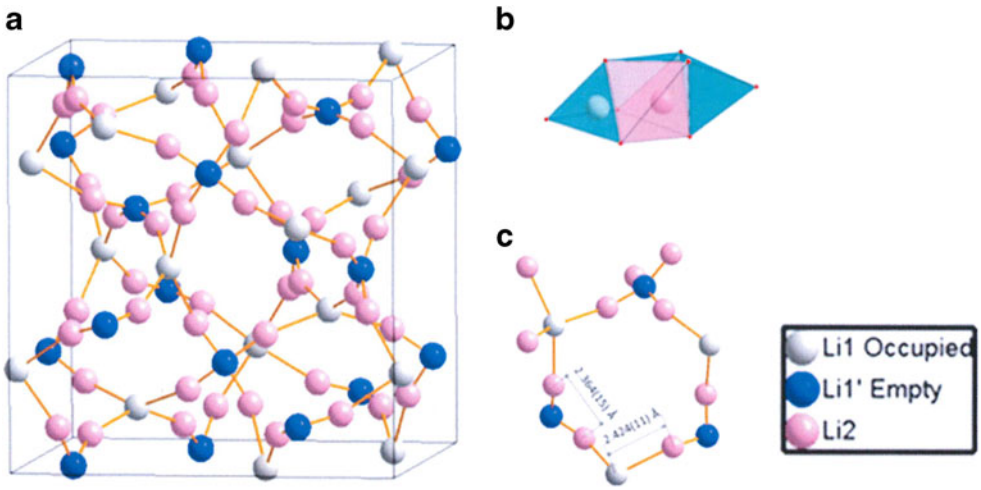

Fig. 12 **a**–**c** Interstitial space of the garnet framework containing 7.5 Li^+ ions/formula unit: *blue*, ordered vacancies on *24 d*; *white*, occupied *24 d* sites; *pink*, octahedral-site Li^+ displaced from *48 g* to *96 h* positions

The cubic garnets $A_3B_3C_2O_{12}$ contain a $B_3C_2O_{12}$ framework of eight coordinated B cations and six coordinated C cations. The interstitial space, shown in Fig. 12, consists of the tetrahedral A cation sites *24 d* of space group *Ia–3d* that are bridged by octahedral sites *48 g* sharing faces on opposite sides with two *24 d* sites. As in the spinel structure, Li^+–Li^+ interactions across a shared face are too strong to permit a Li^+ in a *48 g* site to bridge Li^+ ions in both near-neighbor *24 d* sites. O'Callaghan and Cussen [43] have shown that one of the two neighboring *24 d* sites must be empty and that Li^+–Li^+ interactions across the shared face on the occupied side displaces the octahedral-site Li^+ from the *48 g* position to a *96 h* position close to the opposite face of the octahedron as illustrated in Fig. 12b. It follows that the maximum occupancy of Li^+ in the garnet framework is 7.5 per formula unit and this occupancy is possible only if the vacant interstitial sites are all *24 d* sites ordered as shown in Fig. 12. Firing in an alumina crucible results in adventitious Al^{3+} entering *48 g* sites to create Li^+ ion vacancies and stabilize the structure to a temperature near 1,150 °C with nominal $Li_7La_3Zr_2O_{12}$. A nominal Li^+ ion occupancy at 6.4± 0.1 per formula unit appears to give the highest value of σ_{Li}.

Conclusion

Li ion rechargeable batteries based on liquid-carbonate electrolytes and insertion-compound cathodes have reached a mature stage in which cell capacity is limited by the number of Li^+ guest ions that can be accepted reversibly into the transition metal host structure. This limit is further reduced where the anode μ_A is above the electrolyte LUMO at about 1.1 eV below μ_A (Li^0) because Li^+ ions are incorporated *irreversibly* into an anode-passivating SEI layer on first charge. Moreover, the cathode voltage is restricted by the electrolyte HOMO to be less than 4.5 V versus lithium even if the intrinsic voltage limit imposed by pinning of μ_C at the top of the O-2p bands is lowered to below 4.8 V versus lithium. Realization of a 4.75-V cathode in a carbonate electrolyte requires the formation of a passivating SEI layer on the cathode particles that is stable to volume changes on cycling and is permeable to Li^+ ions. These passivating layers must either be fabricated, as has been demonstrated, or developed intrinsically by suitable doping. Alternatively, a liquid electrolyte having a HOMO > 5.0 eV below μ_A (Li) on the cathode side of a solid Li^+ electrolyte may enable the realization of a specific energy density sufficient for a commercially viable electric vehicle.

Affordable rechargeable stationary batteries for extensive storage of electrical energy feeding the grid await alternative strategies. The fabrication of a robust, thin, flexible Li^+ solid electrolyte separator with a $\sigma_{Li} \simeq 10^{-3}$ S cm^{-1} that can block dendrites from a Li anode represents a challenging new direction that opens up the possibility of new strategies for cells of significant energy density. The ability to replace a Li ion battery with a Na ion battery of comparable performance would lower cost and alleviate concerns about the availability of lithium.

Acknowledgments Financial support of The Robert A. Welch Foundation is gratefully acknowledged.

References

1. Winter M, Brodd RT (2004) What are batteries, fuel cells, and supercapacitors? Chem Rev 104:4245–4269
2. Kummer JT, Weber N (1968) US Patent 3:413–150
3. Lu X, Xia G, Lemmon JP, Yang Z (2010) Advanced materials for sodium-beta alumina batteries: status, challenges, and perspectives. J Power Sources 195:2431–2442
4. Coetzer J (1986) A new high energy density battery system. J Power Sources 18:377–380
5. Xu N, Li X, Zhao X, Huang K, Goodenough JB (2011) A novel battery for grid energy storage. Energy Environ Sci 4:4942–4946
6. Xu K (2004) Nonaqueous liquid electrolytes for lithium-based rechargeable batteries. Chem Rev 10:4303–4417
7. Aurbach D, Gofer Y, Langsam J (1989) The correlation between surface chemistry, surface morphology, and cycling efficiency of lithium electrodes in a few polar aprotic systems. J Electrochem Soc 136:3198–3205
8. Schöllhorn R (1982) Solvated intercalation components of layered chalcogenide and oxide bronzes. In: Whittingham MS, Jacobson AJ (eds) Intercalation chemistry. Academic, New York, pp 315–360
9. J. Rouxel. In: F. Levy (ed) Intercalated layered materials. Reidel, Dordrecht, 1979, pp. 201-250.
10. Whittingham MS (1976) Electrical energy storage and intercalation chemistry. Science 192:1126–1127
11. Mizushima K, Jones PC, Wiseman PJ, Goodenough JB (1980) Li_xCoO_2 ($0<\times\leq 1$): a new cathode material for batteries of high energy density. Mat Res Bull 15:783–789
12. Goodenough JB, Mizushima K, Takeda T (1980) Solid-solution oxides for storage-battery electrodes. Japanese J Appl Phys 19 (Supplement 19-3):305–313
13. Thomas MGSR, Bruce PG, Goodenough JB (1985) Lithium mobility in the layered oxide $Li_{1-x}CoO_2$. Solid State Ionics 17:13–19
14. Bartlett N, McQuillan BW (1982) Graphite chemistry. In: Whittingham MS, Jacobson AJ (eds) Intercalation chemistry. Academic, New York, pp 19–53
15. Yazami R, Touzain Ph (1983) A reversible graphite-lithium negative electrode for electrochemical generators. J Power Sources 9:365–371
16. A. Yoshino (1985) US Patent No. 4, 688, 595 and JP No. 1989293
17. R.V. Chebiam, F. Prado, A. Manthiram. Soft chemistry synthesis and characterization of layered $Li_{1-x}Ni_{1-y}Co_yO_{2-\partial}$ ($0\leq\times\leq 1$ and $0\leq y\leq 1$, **13**, 2951–2957 (2001)
18. Edström K, Gustafsson T, Thomas JO (2004) The cathode–electrolyte interface in the Li-ion battery. Electrochim Acta 50:397–403
19. Yoon S, Manthiram A (2009) Sb–MO_x–C (M=Al, Ti, or Mo) nanocomposite anodes for lithium-ion batteries. Chem Mater 20:3898–3904
20. Goodenough JB, Kim Y (2010) Challenges for rechargeable Li batteries. Chem Mater 22:587–603

21. Goodenough JB (2007) Cathode materials: a personal perspective. J Power Sources 174:196–1000
22. Thackeray MM, David WIF, Goodenough JB (1982) Structural characterization of the lithiated iron oxides $Li_xFe_3O_4$ and $Li_xFe_2O_3$ ($0<\times<2$). Mat Res Bull 17:785–793
23. Thackeray MM, David WIF, Bruce PG, Goodenough JB (1983) Lithium insertion into manganese spinels. Mat Res Bull 18:461–472
24. Thackeray MM, Johnson PJ, de Picciotto LA, Bruce PG, Goodenough JB (1984) Electrochemical extraction of lithium from $LiMn_2O_4$. Mat Res Bull 19:179–187
25. Ferg E, Gummow RJ, de Kock A, Thackeray MM (1994) Spinel anodes for lithium-ion batteries. J Electrochem Soc 141:L147–L150
26. Shin Y, Manthiram A (2003) Influence of lattice parameter difference between the two cubic phases formed in the 4 V region on the capacity fading of spinel manganese oxides. Chem Meter 15:2954–2961
27. Makimura Y, Ohzuku T (2003) Lithium insertion material of $LiNi_{1/2}Mn_{1/2}O_2$ for advanced lithium-ion batteries. J Power Sources 117:156–160
28. Liu D, Han J-T, Dontigny M, Zaqhib K, Goodenough JB (2010) Redox behaviors of ni and cr with different counter cations in spinel cathode for Li-ion batteries. J Electrochem Soc 157: A770
29. Goodenough JB, Hong HY-P, Kafalas JA (1976) Fast Na^+-ion transport in skeleton structures. Mat Res Bull 11:203–220
30. Hong HY-P (1976) Crystal structures and crystal chemistry in the system $Na_{1+x}Zr_2Si_xP_{3-x}O_{12}$. Mat Res Bull 11:173–182
31. Manthiram A, Goodenough JB (1989) Lithium insertion into $Fe_2(SO_4)_3$ frameworks. J Power Sources 26:403–408
32. Padhi AK, Nanjundaswamy KS, Masquelier C, Goodenough JB (1997) Mapping of transition-metal redox couples in phosphates with NASICON structure by lithium intercalation. J Electrochem Soc 144:2581–2586
33. Padhi AK, Nanjundaswamy KS, Goodenough JB (1992) Phospho-olivines as positive electrode materials for rechargeable lithium batteries. J Electrochem Soc 144:1188–1194
34. Zaghib K, Mauger A (2009) Goodenough, J.B., F. Gendron, and C.M Julien. Positive electrode: lithium iron phosphate. In: Garche J, Dyer C, Moseley P, Ogumi Z, Rand D, Scrosati B (eds) Encyclopedia of electrochemical power sources, vol 5. Elsevier, Amsterdam, pp 264–296
35. Ravet N, Goodenough JB, Besner S, Simoneau M, Hovington P, Armand M (1999) Improved iron based cathode material. 196th Electrochemical Society Meeting, Honolulu, Hawaii
36. Zaghib K, Mauger A, Goodenough JB, Julien CM (2011) Design and properties of $LiFePO_4$ nanomaterials for high power applications. In: D. Lockwood (ed) Nanotechnology for Li-ion batteries. Springer, Berlin, 2011, Chap 8
37. Massoun J, Scrosati B (2010) A high-performance polymer tin sulfur lithium ion battery. Angew Chemie 49:2371–2374
38. Freunberger SA, Chen Y, Peng Z, Griffin JM, Hardwick LJ, Bardé F, Novak P, Bruce PG (2011) Reaction in the rechargeable lithium-O_2 battery with alkyl carbonate electrolytes. J Amer Chem Soc 133:8040–8047
39. Wang L, Zhao X, Lu Y, Xu M, Zhang D, Ruoff RS, Stevenson KJ, Goodenough JB (2012) $CoMn_2O_4$ spinel nanoparticles grown on graphene as bifunctional catalyst for lithium-air batteries. J. Electrochem. Soc. (in press).
40. Lu Y, Goodenough JB (2011) Rechargeable alkali-ion cathode-flow battery. J Mater Chem 21:10113–10117
41. Kamaya N, Homma K, Yamakawa Y, Hirayama M, Kanno R, Yonemura M, Kamiyama T, Kato Y, Hama S, Kawamoto K, Mitsui A (2012) A lithium superionic conductor. Nature Materials (in press).
42. Thaugadurai V, Weppener W (2005) J Power Sources 142:399–344
43. O'Callaghan MP, Cussen EJ (2007) Lithium dimer formation in the Li-conducting garnets $Li_{5+x}Ba_xLa_{3-x}Ta_2O_{12}$ ($0<x_{[\leq]}$ 0.16). Chem. Commun. 2048-2050